Effects of Carbon-to-Zeolite Ratio on Layered Bed H_2 PSA for Coke Oven Gas

Chang-Ha Lee, Jaeyoung Yang, and Hyungwoong Ahn
Dept. of Chemical Engineering, Yonsei University, Seoul 120-749, South Korea

Effects of carbon-to-zeolite ratio on a layered bed H_2 PSA using activated carbon and zeolite 5A were studied experimentally and theoretically. Coke oven gas (56.4 vol. % H_2, 26.6 vol. % CH_4, 8.4 vol. % CO, 5.5 vol. % N_2, and 3.1 vol. % CO_2) was used as a feed gas for the seven-step two-bed PSA process incorporating a backfill step. In these experiments, the effects of three operating variables such as adsorption pressure, feed rate and purge rate on the performance of a layered bed PSA were investigated. The layered bed gave better purity than the single-adsorbent bed at the same operating condition, except at low purge rate. Since every component had its own front velocity at each layer, a carbon-to-zeolite ratio affected product purity at a given recovery or throughput. Moreover, for a high-purity H_2 product from coke oven gas, an optimum carbon-to-zeolite ratio had to be determined to control a leading wavefront of N_2. In layered bed PSA processes, the temperature variations inside the bed reflected a kind of inflection or plateau at which a roll-up phenomenon occurred and showed the dynamics of adsorption well at each step during a cycle. Simulated results of the dynamic model incorporating mass, energy and momentum balances agreed well with the PSA experimental results.

Introduction

Increasing demand for hydrogen, particularly in a petroleum refinery and in the petrochemical process, has provided a strong economic motivation to develop a process for recovering hydrogen from refinery fuel gases, coke oven gases (COG), other similar sources, and from more traditional sources such as off-gas (Ruthven et al., 1994; Yang, 1987). In many industrial processes using hydrogen, a high-purity hydrogen product of at least 99.99% is required and higher than 99.999% is often required as well. Since hydrogen is adsorbed much less strongly than almost any other components, a well-designed pressure swing system can meet this challenge. Indeed, this is one application for which pressure swing adsorption (PSA) has a clear advantage over almost all other possible approaches, for many these purity levels are unattainable.

Single-adsorbent H_2 PSA for binary or ternary mixtures with only major impurities have been employed in many previous works (Doong and Yang, 1986; Kumar, 1994; Kim et al., 1995; Yang et al., 1997a,b). However, a practical necessity to obtain a high purity product from a multicomponent feed in commercialized H_2 PSA processes has prompted a simultaneous use of various kinds of adsorbents because different adsorbents show different selectivity depending on the adsorbate. Therefore, an important characteristic of the H_2 PSA process is that many different adsorbents are used either in multiple-layered beds, where each bed is composed of different adsorbents, or in two groups of adsorption beds with different adsorbents. In the typical H_2 PSA with layered beds, the activated carbon layer at the bottom of the bed separates a bulk stream as a separator and the zeolite layer purifies the raffinate stream from the activated carbon separator. Also, the backfill step or product pressurization step in the commercial H_2 PSA has widely been used to increase product purity (Liow and Kenney, 1990; Chou and Huang, 1994).

Correspondence concerning this article should be addressed to C.-H. Lee.
Current address of J. Yang: Sunkyong Engineering and Construction Ltd., Seoul, South Korea.

In spite of the wide utilization of a layered bed H_2 PSA, only a few studies have been done up to now. Kikkinides et al. (1993) and Kumar (1994) studied the influence of adsorbents in a PSA process. Chlendi et al. (1995) investigated a six-step layered bed PSA process to recover H_2 from a pseudo-cracking natural gas, which was carried out by numerical simulation without energy balance and which assumed CO and N_2 as a single component. Recently, Yang and Lee (1998) studied adsorption dynamics of a layered bed using coke oven gas. Through breakthrough experiments and a dynamic model incorporating mass, energy, and momentum balances, they found that controlling a leading wave front of N_2 played a very important role in obtaining a high purity product and the breakthrough times of every component varied with a carbon ratio. They also pointed out there will be an optimum carbon ratio of a layered bed H_2 PSA. In that study, they defined a carbon ratio (c.r.) as a ratio of an activated carbon layer length to a bed length, because the capacity of an adsorbent had to be compared with others under the packing state.

A basic study on the cyclic behavior of a layered bed PSA process is very important in understanding well the performance of the processes under various conditions. In this study, by using a layered bed packed with activated carbon and zeolite 5A, the effects of carbon-to-zeolite ratio on a layered two-bed PSA process with a backfill step were investigated experimentally and theoretically for the H_2 recovery from COG. The effects of various operating variables such as adsorption pressure, feed flow rate, and purge rate on product purity and recovery were also investigated with a change in the carbon ratio of the bed. Then, the results were compared with those of single-adsorbent beds. The experimental results and dynamics of these H_2 PSA processes were predicted by a model simulation, where the effect of operating variables, as well as the optimum carbon-to-zeolite ratio, had all been taken into account.

Mathematical Modeling

A nonisothermal dynamic model including a component balance, overall mass balance, energy balance and momentum balance was used to simulate a PSA process with the following assumptions: (i) the flow pattern in the bed can be described by an axial dispersion plug-flow model; (ii) the intraparticle mass-transfer and adsorption equilibrium can be described by a linear driving force (LDF) model and Langmuir-Freundlich (L-F) model, respectively; (iii) the solid and gas phases reach thermal equilibrium instantaneously; (iv) radial concentration and temperature gradients in the adsorption bed are negligible; (v) axial conduction in the wall can be neglected; (vi) the gas phase behaves as an ideal gas mixture.

Using an axially dispersed plug flow and an ideal gas law, the material balance for the bulk phase in the adsorption column was given by

$$-D_L\frac{\partial^2 y_i}{\partial z^2}+\frac{\partial y_i}{\partial t}+u\frac{\partial y_i}{\partial z}+\frac{RT}{P}\frac{1-\epsilon}{\epsilon}\rho_p\left(\frac{\partial \bar{q}_i}{\partial t}-y_i\sum_{j=1}^{n}\frac{\partial \bar{q}_j}{\partial t}\right)=0 \quad (1)$$

and the overall mass balance was represented as follows

$$-D_L\frac{\partial^2 P}{\partial z^2}+\frac{\partial P}{\partial t}+P\frac{\partial u}{\partial z}+u\frac{\partial P}{\partial z}+PT\left[-D_L\frac{\partial^2}{\partial z^2}\left(\frac{1}{T}\right)+\frac{\partial}{\partial t}\left(\frac{1}{T}\right)+u\frac{\partial}{\partial z}\left(\frac{1}{T}\right)\right]-2D_LT\frac{\partial}{\partial z}\left(\frac{1}{T}\right)\frac{\partial P}{\partial z}+\frac{1-\epsilon}{\epsilon}\rho_p RT\sum_{j=1}^{n}\frac{\partial \bar{q}_j}{\partial t}=0 \quad (2)$$

Assuming a thermal equilibrium between fluid and particles, the energy balance for gas and solid phases was given by

$$-K_L\frac{\partial^2 T}{\partial z^2}+\left(\alpha\rho_g(C_p)_g+\rho_B(C_p)_s\right)\frac{\partial T}{\partial t}+\rho_g(C_p)_g\epsilon u\frac{\partial T}{\partial z}-\rho_B\sum_i^n Q_i\frac{\partial \bar{q}_i}{\partial t}+\frac{2h_i}{R_{B_i}}(T-T_w)=0 \quad (3)$$

where K_L is the effective axial thermal conductivity (J/m·s·K) (Suzuki, 1990; Malek and Farooq, 1997).

Since the diameter of the adsorption bed used in the present study was rather small, the heat loss through a wall and heat accumulation in the wall could not be neglected. Therefore, another energy balance for the wall of the adsorption bed was used by neglecting the axial conduction in the wall.

$$\rho_w(C_p)_w A_w\frac{\partial T_w}{\partial t}=2\pi R_{Bi}h_i(T-T_w)-2\pi R_{Bo}h_o(T_w-T_{atm}) \quad (4a)$$

$$A_w=\pi\left(R_{Bo}^2-R_{Bi}^2\right) \quad (4b)$$

The Ergun's equation shown below was applied to the pressure drop across the bed (Lu et al., 1993; Yang et al., 1998)

$$-\frac{dP}{dz}=a\mu\nu+b\rho\nu|\nu| \quad (5a)$$

$$a=\frac{150}{4R_p^2}\frac{(1-\epsilon)^2}{\epsilon^3},\qquad b=1.75\frac{(1-\epsilon)}{2R_p\epsilon^3} \quad (5b)$$

where ν is superficial velocity (m/s).

The sorption rate into an adsorbent pellet was described by the following LDF model, with a single lumped mass-transfer parameter ω (s^{-1}) (Ruthven et al., 1994)

$$\frac{\partial \bar{q}_i}{\partial t}=\omega_i\left(q_i^*-\bar{q}_i\right) \quad (6)$$

The well-known Danckwerts boundary conditions were applied to the steps which have influent streams. The boundary conditions used in the PSA simulation were in the following forms:

Boundary Conditions for Feed Pressurization and Adsorption Steps

$$-D_L\left(\frac{\partial y_i}{\partial z}\right)\Big|_{z=0} = u\left(y_i|_{z=0^-} - y_i|_{z=0^+}\right); \qquad \left(\frac{\partial y_i}{\partial z}\right)\Big|_{z=L} = 0 \quad (7a)$$

$$-K_L\left(\frac{\partial T}{\partial z}\right)\Big|_{z=0} = \rho_g\left(C_p\right)_g u\left(T|_{z=0^-} - T|_{z=0^+}\right); \qquad \left(\frac{\partial T}{\partial z}\right)\Big|_{z=L} = 0 \quad (7b)$$

where $y_i|_{z=0^-}$ means feed composition for component i.

Boundary Conditions for Purge, Pressurizing Pressure Equalization, and Backfill Steps

$$-D_L\left(\frac{\partial y_i}{\partial z}\right)\Big|_{z=L} = u\left(y_i|_{z=L^+} - y_i|_{z=L^-}\right); \qquad \left(\frac{\partial y_i}{\partial z}\right)\Big|_{z=0} = 0 \quad (8a)$$

$$-K_L\left(\frac{\partial T}{\partial z}\right)\Big|_{z=L} = \rho_g\left(C_p\right)_g u\left(T|_{z=L^+} - T|_{z=L^-}\right); \qquad \left(\frac{\partial T}{\partial z}\right)\Big|_{z=0} = 0 \quad (8b)$$

where $y_i|_{z=L^+}$ means a volume-averaged composition of the effluent stream during the adsorption step for purge and backfill steps, and a temporal effluent stream's composition during a depressurizing pressure equalization step for the pressurizing pressure equalization step, respectively. The fluid velocity is inherently negative during these steps.

Boundary Conditions for Depressurizing Pressure Equalization and Countercurrent Depressurization Steps

$$\left(\frac{\partial y_i}{\partial z}\right)_{z=0} = \left(\frac{\partial T}{\partial z}\right)_{z=0} = 0; \qquad \left(\frac{\partial y_i}{\partial z}\right)_{z=L} = \left(\frac{\partial T}{\partial z}\right)_{z=L} = 0 \quad (9)$$

The equilibrium of mixtures was predicted by following the extended Langmuir-Freundlich model

$$q_i = \frac{q_{mi} B_i P_i^{n_i}}{1 + \sum_{j=1}^{n} B_j P_j^{n_j}} \quad (10a)$$

$$q_m = k_1 + k_2 T, \qquad B = k_3 e^{k_4/T}, \qquad n = k_5 + k_6/T \quad (10b)$$

The axial dispersion coefficient D_L (m^2/s) was calculated by a Wakao equation using interstitial feed velocity at the adsorption pressure and this constant value was used for all the steps (Wakao and Funazkri, 1978)

$$\frac{D_L}{2uR_p} = \frac{20}{ReSc} + 0.5 \quad (11)$$

The effective axial thermal conductivity K_L was used by the following empirical correlation (Yagi et al., 1960; Kunii and Smith, 1960; Suzuki, 1990) instead of the axial thermal dispersion coefficient (Yang et al., 1997b)

$$K_L/k_g = K_{L0}/k_g + \delta\, Pr Re \quad (12a)$$

$$K_{L0}/k_g = \epsilon + \frac{1-\epsilon}{\phi + (2/3)\left(k_g/k_s\right)} \quad (12b)$$

$$\phi = \phi_2 + (\phi_1 - \phi_2)\left(\frac{\epsilon - 0.26}{0.216}\right) \text{ for } 0.260 \le \epsilon \le 0.476 \quad (12c)$$

The bed porosities for activated carbon and zeolite 5A beds were both within the range of Eq. 12c, as shown in Table 1. Three parameters (δ, ϕ_1, and ϕ_2) of these equations for both activated carbon bed and zeolite 5A bed were 0.75, 0.2, and 0.1, respectively (Suzuki, 1990). The constant effective axial thermal conductivity, which was estimated by using Eq. 12 under the experimental condition of the adsorption step, was used for the simulation of that run.

For input parameters of model simulation, the adsorption isotherm data and the sorption rate by a linear driving force (LDF) model of CH_4, CO, N_2, CO_2, and H_2 on the activated carbon and zeolite 5A were the same as those in the previous work (Yang and Lee, 1998). The isosteric heat of adsorption for each adsorbate-adsorbent pair was calculated by using a Clausius-Clapeyron equation (Yang et al., 1997b).

To develop a mathematical model for a layered bed, it was assumed that a double layered bed consisted of two single-adsorbent beds linked in series. This mathematical model and numerical simulation for a layered bed PSA process were described elsewhere in details (Yang and Lee, 1998).

Experimental Studies

The COG feed used in this study was H_2 (56.4 vol. %) mixture gas with CH_4 (26.6 vol. %), CO (8.4 vol. %), N_2 (5.5

Table 1. Characteristics of Adsorption Bed and Adsorbents

Adsorption Bed		
Length	100 cm	
Inside diameter	3.71 cm	
Outside diameter	4.245 cm	
Heat capacity of wall	0.12 cal/g·K	
	Activated Carbon Bed	Zeolite Bed
Bulk (bed) density	0.482 g/cm^3	0.764 g/cm^3
External void fraction	0.433	0.357
Total void fraction	0.78	0.77
Adsorbents		
	Activated Carbon	Zeolite 5A
Pellet size	6–16 mesh	4–8 mesh
Pellet density	0.85 g/cm^3	1.16 g/cm^3
Heat capacity	0.25 cal/g·K	0.22 cal/g·K

vol. %), and CO_2 (3.1 vol. %) purchased from a gas company (Daesung Sanso Co., South Korea).

The adsorption beds were 100 cm long and 3.71 cm I.D. Four resistance temperature detectors (RTD, Pt 100Ω) were installed at the positions of 10, 30, 50, and 75 cm from the feed end to measure temperature variations inside the adsorption bed. For layered bed experiments, the activated carbon (PCB, 6–16 mesh) manufactured by Calgon Carbon Co. (U.S.A.) was packed into the bottom of the bed, because a zeolite 5A is almost saturated with CO_2 at low pressure. Then, after putting a metal screen of 0.3 mm thickness on top of the activated carbon layer, zeolite 5A (4–8 mesh) manufactured by W. R. Grace Co. (U.S.A.) was added. The characteristics of the bed and adsorbents are shown in Table 1.

Feed and purge flow rates were controlled by mass-flow controllers (Bronkhorst high-tech, F-201C). To calculate recovery accurately, the amount of gas flowing into and out of the PSA system was measured with a mass-flow meter (Bronkhorst high-tech, F-112ac-HA-55-V) and a wet gas meter (Shinagawa, W-NK-1B). Gas samples taken from a product tank were analyzed by using a mass spectrometer (Balzers, QME 200) and a GC (HP, GC 5890 II) for N_2 and CO. The PSA system was fully automated by interfacing with a personal computer and all the measured data were saved on the computer. The details for the system are described in Yang and Lee's (1998) study.

The following cycle sequence and step time for this two-bed seven-step PSA process were used: (1) feed pressurization of a partially pressurized bed by a previous pressurizing pressure equalization (FP: 4s); (2) high-pressure adsorption (AD: 180s); (3) depressurizing pressure equalization (DPE: 20s); (4) countercurrent depressurization (DP: 8s); (5) purge with a light product, H_2 (PG: 180s); (6) pressurizing pressure equalization (PPE: 20s); (7) a backfill step with light product up to the average pressure of the adsorption pressure and final pressure of pressurizing pressure equalization (BF: 4s). The effluent in step II (AD) is high purity H_2 product and this experimental and theoretical study concentrated upon the quality and quantity of this light product rather than those of heavy product.

Results and Discussion

Cyclic steady state of PSA process

Figure 1 showed a representative cyclic behavior of a layered bed PSA process, plotting a simulated composition variation of effluent stream from the adsorption bed with time. The hydrogen concentration of the effluent was obtained from the product end during the adsorption step and depressurizing pressure equalization step. And, it was also obtained from the feed end during the countercurrent depressurization step and purge step.

In the case of the frozen solid-phase model, it was impossible to predict a transient variation of the effluent stream during pressurization and depressurization steps because the solid-phase concentration was assumed to remain unchanged at the end of the previous step (Farooq et al., 1988; Lu et al., 1993). However, the LDF model used in the present study showed a reasonable prediction of effluent composition for all the steps in Figure 1. The composition of the effluent stream approached rapidly to a cyclic steady state as shown

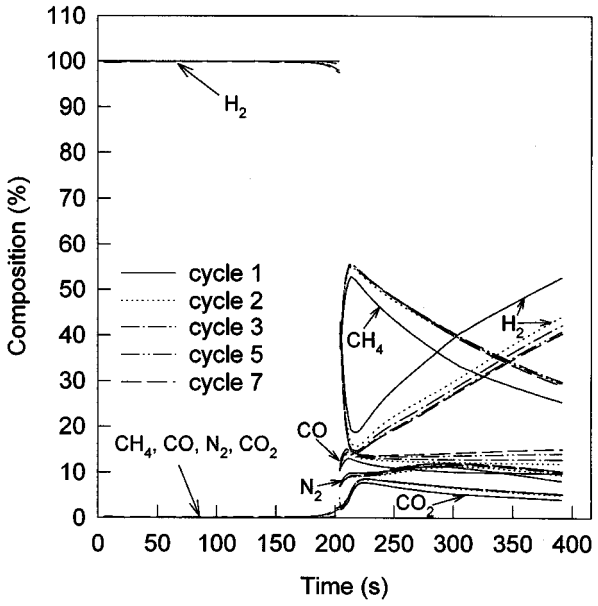

Figure 1. Cyclic approach of gas composition of effluent stream to dynamic steady state in a layered bed process with 0.65 carbon-to-zeolite ratio under 10 atm adsorption pressure, 8 LSTP/min feed rate, and 0.7 LSTP/min purge rate.

in this figure. After approximately 10 cycles, the difference between the performance of the last two cycles was less than 0.01 %. And, it was also confirmed by the 25-cycle PSA experiments and 100-cycle simulations. In the present study, all the experimental data were collected at above 15 cycles.

In Figure 1, constant purity product at the adsorption step after a cyclic steady state was obtained because the operating conditions were favorable. During the depressurizing pressure equalization step (DPE), the emitting gases from the product end of the adsorption bed with a steep decrease in total pressure made concentration wavefronts disperse and proceed quickly. Also, this step made the adsorbed components desorb and led to a decrease in H_2 mole fraction of effluent stream as shown in Figure 1. However, Yang et al. (1997b) pointed out that a decrease in H_2 concentration of effluent stream during the DPE step contaminated the product end and had a bad effect on product purity. Therefore, the product purity at this step was not high due to the unfavorable operating condition. At the countercurrent depressurization step, the rapid decrease in total pressure led to further desorption of the adsorbed components and an increase in mole fraction of strongly adsorbed components in an effluent stream. Also, desorption continued at the purge step. Therefore, the composition of strongly adsorbed components rose at the early stage of a purge step until the influent stream of higher purity H_2 reached the feed end. The dynamics of each step in the layered bed PSA process will be explained later in detail.

Along with the concentration of the effluent stream, the temperature variation inside the adsorption bed represented a cyclic behavior of a PSA process. The temperature variations at four locations along the layered bed with 0.65 car-

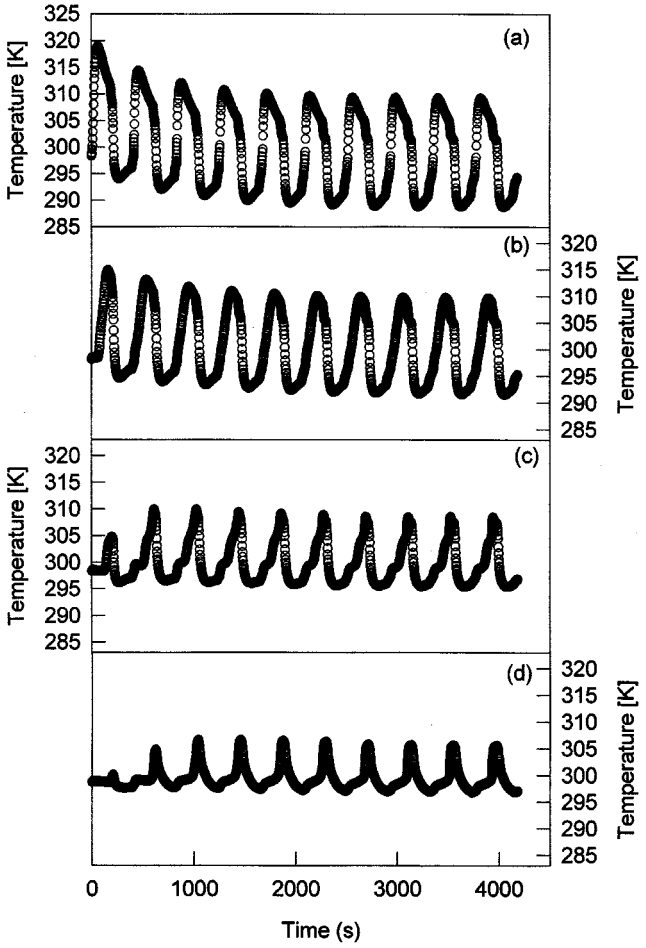

Figure 2. Transient variation of temperature at (a) $z = 10$ cm, (b) $z=30$ cm, (c) $z=50$ cm, and (d) $z=75$ cm for a layered bed process with 0.65 carbon-to-zeolite ratio under 10 atm adsorption pressure, 8 LTP/min feed rate, and 0.7 LTP/min purge rate.

bon-to-zeolite ratio were presented in Figure 2. It could be seen that a PSA process approached rapidly a cyclic steady state as revealed by the predicted concentration of an effluent stream (Figure 1). The range of temperature swing was largest at the feed end section, because this section behaved as a separator where a considerable amount of adsorbates underwent adsorption and desorption during a cycle. However, the range of temperature swing at the product end section was smallest because this section purified the raffinate stream from the activated carbon separator. It was noteworthy that the two temperature sensors of 50 and 75 cm at the initial cycles showed relatively little extent of temperature swing. This implied that, at an early stage of operation, the concentration wavefronts did not proceed much from feed end due to the initial condition of the clean bed.

Effects of adsorption pressure and carbon-to-zeolite ratio

To study the effect of carbon-to-zeolite ratio of a layered bed in detail, many PSA runs were experimented by using

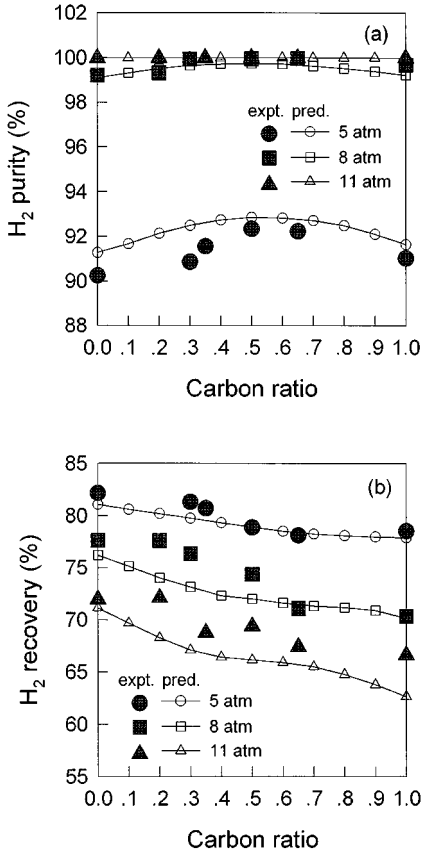

Figure 3. Effect of carbon ratio on (a) purity and (b) recovery at three adsorption pressures, 7 LSTP/min feed rate, and 0.7 LSTP/min purge rate.

adsorption beds with various carbon-to-zeolite ratios under three different adsorption pressures. As shown in Figure 3a and Table 2, there existed a carbon-to-zeolite ratio which gave the highest product purity at each adsorption pressure. Also, the purity difference upon carbon-to-zeolite ratio appeared much less sharp as adsorption pressure increased. At 5 atm adsorption pressure, the layered bed with around 0.5 carbon-to-zeolite ratio gave best product purity and the activated carbon bed gave higher purity than the zeolite bed. At this adsorption pressure, the reason for purity change by carbon ratio was explained in Figure 4. While the main impurities in the H_2 product of the processes using zeolite-rich bed were

Table 2. H_2 Product Purity and Recovery Under 11 atm Adsorption Pressure, 7 LSTP/min Feed Rate and 0.7 LSTP/min Purge Rate

Carbon-to-Zeolite Ratio	0.0	0.2	0.35	0.5	0.65	1.0
H_2 Purity (%)	99.983 (99.986)	99.986 (99.987)	99.985 (99.988)	99.991 (99.999)	99.981 (99.995)	99.988 (99.978)
H_2 Recovery (%)	71.96 (71.13)	72.09 (68.25)	68.75 (67.10)	69.38 (66.15)	66.62 (65.74)	66.62 (62.66)

Simulated results are in parentheses.

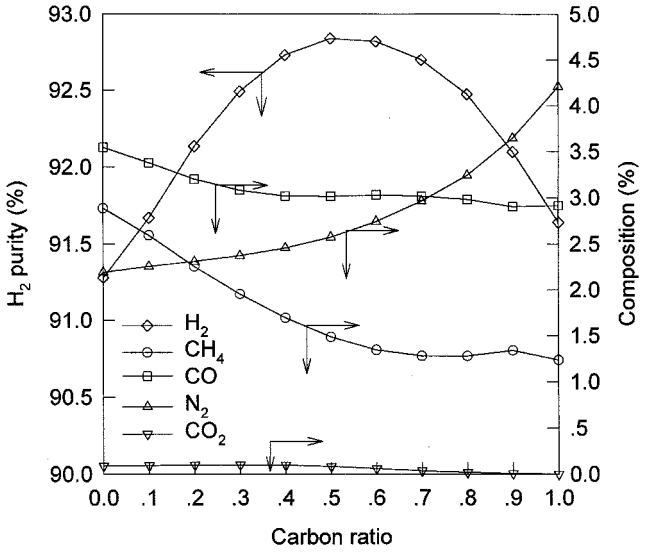

Figure 4. Average composition variation of products with carbon ratio under 5 atm adsorption pressure, 7 LSTP/min feed rate, and 0.7 LSTP/min purge rate.

CH_4 and CO, N_2 became a major impurity in a product as carbon-to-zeolite ratio increased. Although the adsorption pressure was different and the adsorption bed was not clean in a cyclic PSA process, this result agreed well with that obtained from breakthrough experiments (Yang and Lee, 1998). Due to the adsorption capacity of the activated carbon bed for CH_4, the breakthrough time of CH_4 was longer than that of CO and N_2. Therefore, CH_4 did not act as one of main impurities for an activated carbon-bed process. On the other hand, in the case of a zeolite bed, CH_4 breakthrough time was comparable with that of CO and N_2. Therefore, CH_4 could be one of the main impurities in a zeolite bed process, especially when the adsorption pressure was low. As a result, the carbon-to-zeolite ratio to improve H_2 purity moved to a low carbon-to-zeolite ratio as N_2 composition in the feed increased. On the other hand, the carbon-to-zeolite ratio for the high H_2 purity moved to high carbon-to-zeolite ratio as the composition of CH_4 and CO in a product increased.

However, in the case of 8 atm adsorption pressure, the simulated result in Figure 3a showed that the carbon ratio for the highest product purity shifted a little to low carbon ratio in comparison with the 5 atm case. At this condition, even in a zeolite bed process, the major impurity became N_2 with a relatively small amount of CO instead of CH_4. Since the increased adsorption capacity for CH_4 and CO with an increase in the adsorption pressure was relatively higher than that for N_2, the importance of CH_4 and CO in product purity became small. Even though the effect of carbon-to-zeolite ratio on purity was not clearly shown for the 11 atm case in Figure 3a, this effect played an important role in obtaining high purity in H_2 product ($> 99.99+\%$) from COG by a PSA process. The role of a layered bed in the PSA process was clearly shown in Table 2, which represented a performance comparison of activated carbon, zeolite and layered beds. As shown in this table, it was very hard to obtain more than 99.99% H_2 purity product even at 11 atm by a single-adsorbed bed process. The carbon-to-zeolite ratio to obtain the highest purity at 11 atm was between 0.35 and 0.5, experimentally, and between 0.4 and 0.5, theoretically, giving $99.991+\%$ and 99.999% H_2 purity, respectively.

In Figure 3b, the recovery of H_2 product showed an inflectional decrease with increasing carbon-to-zeolite ratio at each adsorption pressure, especially at low adsorption pressure. The recovery in the range of 0.4–0.6 carbon-to-zeolite ratio which gave the highest product purity at a given adsorption pressure was higher than those of the activated carbon-rich bed processes which gave lower product purity under the same condition. Also, in single-adsorbent bed processes that gave similar product purity, the recovery at the zeolite bed process was higher than that at the activated carbon bed process and the difference in recovery between two single-adsorbent bed processes increased with an increase in the adsorption pressure.

Through a simulation at higher than 11 atm adsorption pressure, it was found that recovery decreased more steeply and purity approached more slowly to the desired product purity ($99.99+\%$) by increasing adsorption pressure in a zeolite bed process than in any other bed processes. Therefore, at higher than 99.99% H_2 purity from COG, a layered bed PSA proved to be better than activated carbon or zeolite 5A bed PSA in respect to H_2 recovery.

Effects of feed rate and carbon-to-zeolite ratio

The effect of feed rate on the performance of a PSA process was studied with varying carbon ratio under the adsorption pressure of 11 atm and the purge rate of 0.7 L STP/min. Considering the adsorption capacity of a given adsorption bed, the effect of increasing feed rate was basically the same as that of decreasing adsorption pressure. As shown in Figure 5a, the H_2 purity curve had a plateau at some carbon ratio range and then declined. The carbon-to-zeolite ratio to obtain the highest purity under 10 LSTP/min feed was between 0.5 and 0.8. However, this ratio for purity moved to the left as the feed rate was reduced. For PSA processes with 10 LSTP/min feed rate, the effect of carbon-to-zeolite ratio on purity was prominent at low values. Therefore, it could be said that activated carbon played a very important role in controlling the extent of breakthroughs of major impurities over low carbon-to-zeolite ratio range of the adsorption bed. Also, compared to zeolite, activated carbon had larger adsorption capacity for CH_4 per unit volume of an adsorption bed. Also, the adsorption capacity of activated carbon for CO was slightly larger than that of zeolite 5A at higher than 5 atm adsorption pressure. Therefore, with an increase in feed rate, the H_2 purity in the activated carbon bed process dropped less than that in the zeolite bed process.

As expected, the zeolite bed gave the highest recovery at each feed rate condition in Figure 5b, which was similar to the effect of the adsorption pressure mentioned earlier. However, at higher than 99.99% H_2 purity, the layered bed PSA gave the highest recovery of H_2 like the results mentioned in the previous section. In general, experimental results gave higher recoveries than simulated results and a maximum of 4% error was found at 7 and 8 LSTP/min feed rates.

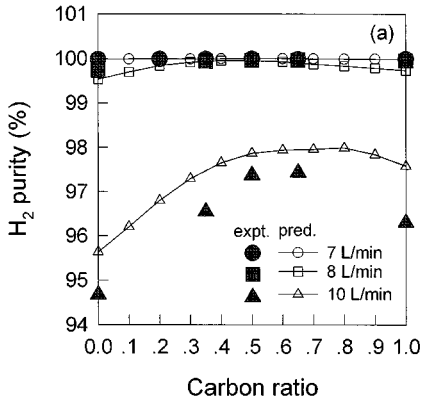

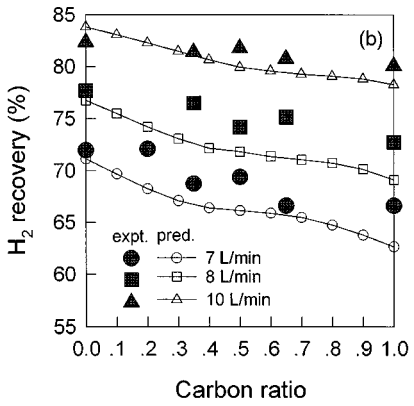

Figure 5. Effects of carbon ratio on (a) purity and (b) recovery at three feed rates, 11 atm adsorption pressure, and 0.7 LSTP/min purge rate.

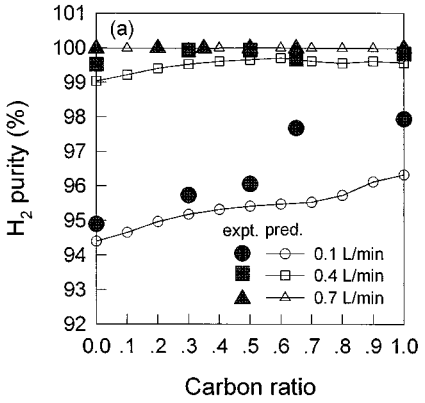

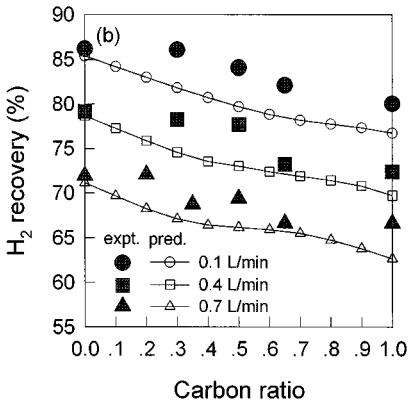

Figure 6. Effects of carbon ratio on (a) purity and (b) recovery at three purge rates, 11 atm adsorption pressure and 7 LSTP/min feed rate.

Effect of purge rate and carbon-to-zeolite ratio

Unlike the above two cases, the effects of carbon-to-zeolite ratio with various purge rates on PSA performance were rather complicated. As shown in Figure 6, at low purge rate, 0.1 LSTP/min, the activated carbon bed gave the best H_2 purity. Under the condition of the pressure swinging from 1 atm to 11 atm, the working capacity of the activated carbon bed, especially for CH_4, was larger than that of the zeolite 5A bed (Yang and Lee, 1998). Therefore, the activated carbon bed could be regenerated in some measure by the depressurization step itself. However, to acquire the needed working capacity for the next cycle, partial pressure of a strongly adsorbed component during a purge step needed to be reduced more in the zeolite 5A bed than in the activated carbon bed. Therefore, the effect of the purge step with low purge rate on the activated carbon-rich bed was greater than that on the zeolite-rich bed. However, in Figure 6a, the improvement of purity in the zeolite-rich bed with an increase in purge rate was higher than that in the activated carbon-rich bed. The reason was that the concentration wavefronts of impurities in the layered bed by an incomplete purge of strongly adsorbed components under a high purge rate became similar to those of the activated carbon bed and the product end of the layered bed was kept cleaner than that of the activated carbon bed. As a result, the highest product purity at 0.7 LSTP/min was obtained from around 0.5 carbon ratio bed due to the adsorption capacity of the zeolite layer for N_2.

In Figure 6b, for recovery, all the experimental data resulted in slightly higher recovery than predicted. Also, the zeolite bed at each purge rate condition was better than any other beds like the results of the adsorption pressure and the feed rate. However, at high H_2 purity (99.99+%) similar recovery results were obtained as in the previous operating variables.

Effects of carbon-to-zeolite ratio on layered bed dynamics

It was noted that the layered bed gave higher product purity than two single-adsorbent beds at the same operating condition. This meant that the carbon-to-zeolite ratio to obtain the highest purity was present under the same operating condition. To clarify the fact, concentration profiles in the gas phases at the end of the adsorption step were presented in Figure 7 for three different layered beds. As shown in this figure, although CH_4 was a major impurity gas in the feed, the most important components in the H_2 PSA process for COG were CO and N_2. Because the adsorption capacity of activated carbon for N_2 was less than that of zeolite 5A, N_2 became a major impurity in the product stream when carbon-to-zeolite ratio was increased.

In Figure 7a, a small but broad roll-up of CH_4 was shown due to the competitive adsorption with a more strongly ad-

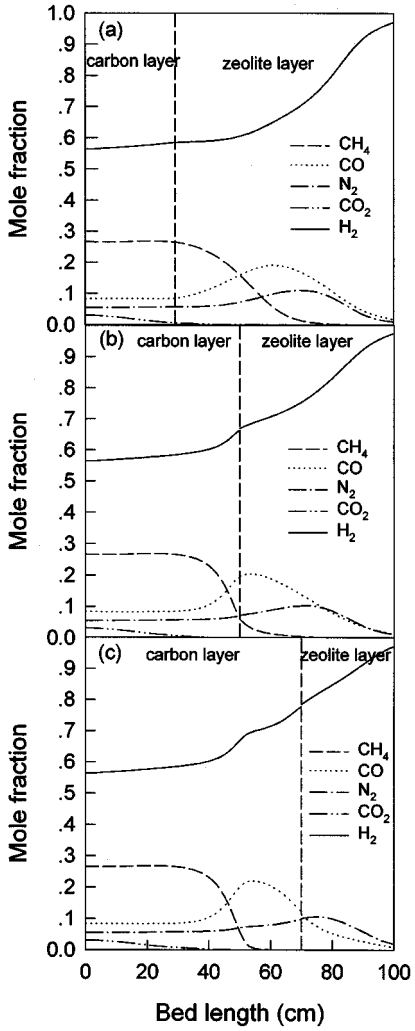

Figure 7. Concentration profiles at a cyclic steady state for layered bed processes with (a) 0.2, (b) 0.5, and (c) 0.7 carbon-to-zeolite ratio at the end of the adsorption step under 7 atm adsorption pressure, 7 LSTP/min feed rate, and 0.7 LSTP/min purge rate.

sorbed component CO_2. Particularly, the concentration profile of CO_2 passing over the activated carbon layer gave detrimental effects on the zeolite layer due to the strong adsorption of CO_2. Therefore, the product stream of zeolite-rich bed contained much CO as well as N_2 because the dispersed and advanced wavefront of CH_4 pushed forward the CO wavefront.

The layered bed with increased carbon ratio could eliminate the above disadvantages of the zeolite-rich bed by imposing on each layer a different role. Namely, while activated carbon adsorbed mainly CH_4, zeolite 5A adsorbed CO and N_2. The corresponding concentration profiles of a layered bed with a 0.5 carbon-to-zeolite ratio were shown in Figure 7b. This layered bed eliminated, in some measure, the disadvantages of a zeolite-rich bed. However, the forefront of the CH_4 wavefront still caused a negative effect on a zeolite layer. Therefore, in order to protect the zeolite 5A layer from the CH_4 wavefront, the carbon-to-zeolite ratio was increased to 0.7 and the results were presented in Figure 7c. According to the increased carbon-to-zeolite ratio, the wavefront of CH_4 remained in the carbon layer and the other part of the adsorption bed could be used to adsorb CO. Therefore, in the product stream, the composition of CO can be reduced with an increase of N_2 composition because the fast and dispersed MTZ of CO led to a long leading front on the N_2 wave front. Such behavior of wavefronts might become more complicated at lower adsorption pressure, because the CH_4 wavefront did not any longer only reside in a carbon layer and was mixed with CO and N_2 wavefronts. As a result, it was very important to find out the superposing configuration of adsorbents to obtain high product purity at a given recovery.

Along with concentration profiles inside the adsorption bed, the temperature variations with time were also useful in understanding the effect of carbon-to-zeolite ratio on bed dynamics. Experimental temperature variations with time at four locations along the bed under 11 atm adsorption pressure, 7 LSTD/min feed rate, and 0.7 LSTD/min were presented with the simulated results in Figure 8–10. The temperature variations in these figures reflected a kind of inflection or plateau at which a roll-up phenomenon occurred as in Figure 7.

In the case of the activated carbon bed process shown in Figure 8a, an abrupt rise of temperature at a short feed pressurization step was followed by a successive rise and drop of temperature from the feed end at the adsorption step. This was because of the propagation of distinctive concentration wavefronts mentioned in Figure 7. However, in the zeolite bed process, the temperature excursion at the adsorption step was continuously increased up to the third RTD. Since the dispersed and advanced wavefront of CH_4 by CO_2 pushed forward the CO wavefront at the adsorption step in the zeolite bed process, mass-transfer zones of N_2 and CO were mixed at the product end section. According to this, the highest-temperature excursion in the zeolite bed occurred near the third RTD position and was sharper than that in the activated carbon bed.

During the depressurizing pressure equalization step, Figure 8 showed that the temperatures in both single-adsorbent beds dropped because of the endothermic desorption. This implied that some amount of adsorbates adsorbed during the feed pressurization and adsorption steps was desorbed at this step. The temperatures in both single-adsorbent bed processes dropped significantly during the countercurrent depressurization step and at the beginning of the purge step. However, after this temperature decrease, a small temperature rise in the activated carbon bed was shown at the purge step. It was due to the heating by the purge gas, which was around 292 K. During the pressurizing pressure equalization step, temperature rose again in both single-adsorbent beds.

Experimental temperature variations for the zeolite bed in Figure 8b showed some discrepancy with the simulated one. Especially, the temperatures showed a relatively slow and small decrease during the countercurrent depressurization step and at the beginning of the purge step. Also, the experimental temperatures during the purge step decreased continuously, which was different from the activated carbon bed. This is possibly because of the slow desorption at the purge step and the dispersed wavefronts of the adsorbates remain-

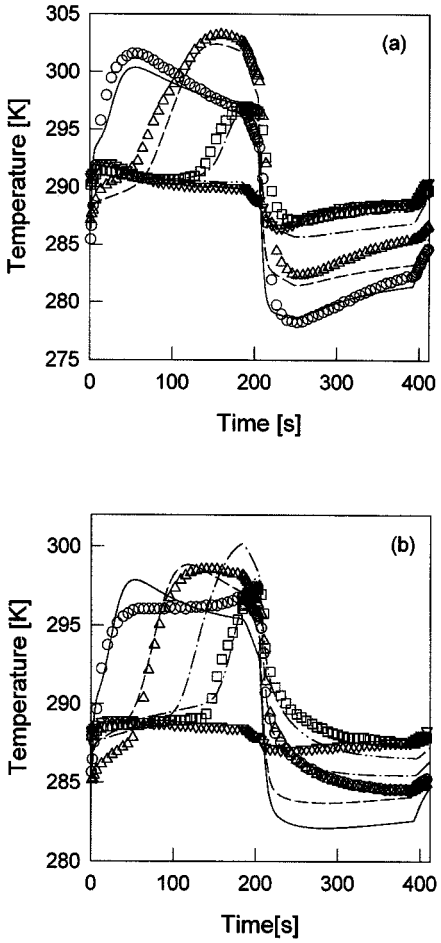

Figure 8. Temperature variations at a cyclic steady state for single-adsorbent bed PSA processes with (a) activated carbon and (b) zeolite 5A under 11 atm adsorption pressure, 7 LSTP/min feed rate, and 0.7 LSTP/min purge rate.

Expt.: ○ 10 cm, △ 30 cm, □ 50 cm, ▽ 75 cm; Pred.: —— 10 cm, – – – 30 cm, –·–·– 50 cm, –··–··– 75 cm.

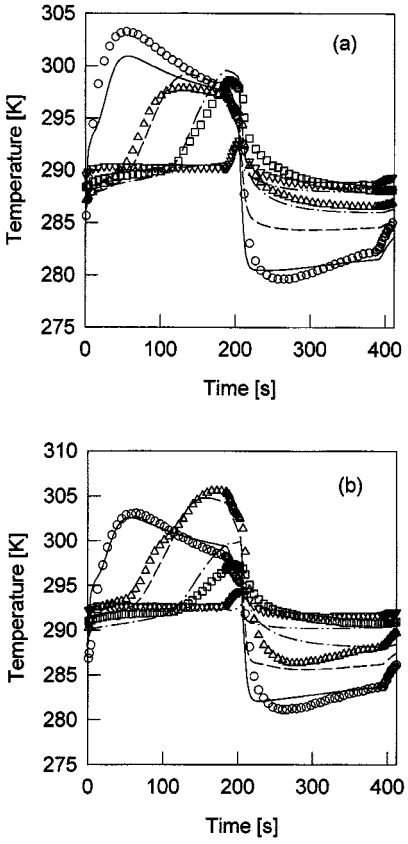

Figure 9. Temperature variations at a cyclic steady state for layered bed PSA processes with (a) 0.2 and (b) 0.3 carbon-to-zeolite ratio under 11 atm adsorption pressure, 7 LSTP/min feed rate and 0.7 LSTP/min purge rate.

Expt.: ○ 10 cm, △ 30 cm, □ 50 cm, ▽ 75 cm; Pred.: —— 10 cm, – – – 30 cm, –·–·– 50 cm, –··–··– 75 cm.

ing in the bed after the regeneration steps. Also, since the temperature in the bed during the desorption steps was not less than that of the atmosphere, there was no effect of heat input from the surroundings. As a result, insufficient regeneration affected the adsorption and depressurizing pressure equalization steps which also showed some discrepancy between experimental and simulated results.

Figures 9 and 10 showed temperature variations for each layered bed process with a different carbon-to-zeolite ratio. The layered bed process with low carbon-to-zeolite ratio showed quite different temperature variations from the zeolite bed process due to different concentration wavefronts of strong adsorbates in the activated carbon layer. As shown in Figure 9a, an abrupt rise of temperature in the feed end occurred due to the adsorption of strong adsorbates at a short feed pressurization step. Then, the temperature excursion of the second RTD (zeolite layer) from the feed end was smaller than that in the activated carbon layer because the adsorption capacity of zeolite 5A for CH_4 and CO was smaller than that on the activated carbon. Also, the temperatures in the position of second and third RTDs from the feed end were continuously increased until the depressurizing pressure equalization step, which was due to the dispersed concentration wavefronts of CH_4 and CO in the zeolite layer. However, with increased carbon-to-zeolite ratio, the temperature variations of the layered bed process became similar to those of the activated carbon bed process.

In Figures 9 and 10, during the depressurizing pressure equalization step, the two temperature profiles at the product end rose because of the fast movement of wavefronts, while the two temperatures at the feed end dropped. At that step, the zeolite-rich bed process showed sharper temperature excursion than the activated carbon-rich bed process due to the roll-up of CH_4 at the product end. However, the layered bed process with 0.5 carbon-to-zeolite ratio in Figure 10a showed much smaller temperature excursion at that step than any other layered bed processes. Especially, the temperature variations for this layered bed process show an intermediate behavior of the single-adsorbent bed process shown in Figure 8. While the temperature variations of two RTDs in the feed end at all steps were very similar to those of the

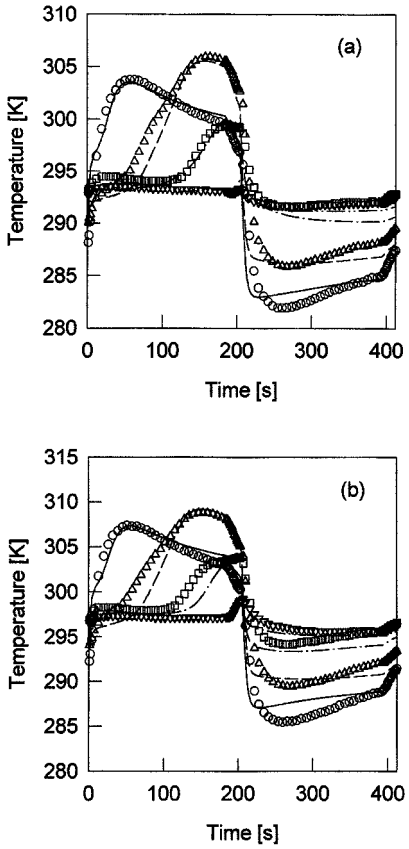

Figure 10. Temperature variations at a cyclic steady state for layered bed PSA processes with (a) 0.5 and (b) 0.65 carbon-to-zeolite ratio under 11 atm adsorption pressure, 7 LSTP/min feed rate, and 0.7 LSTP/min purge rate.

Expt.: ○ 10 cm, △ 30 cm, □ 50 cm, ▽ 75 cm; Pred.: —— 10 cm, – – – 30 cm, –·–·– 50 cm, –··–··– 75 cm.

activated carbon bed process, the temperature variation in the product end was similar to that of the zeolite bed process mainly due to the adsorption of nitrogen. As a result, the layered bed process with this carbon-to-zeolite ratio could give better product purity than any other process at that operating condition. This was because the product end of this layered bed was contaminated less by the N_2 wavefront than that of other processes. This result for the highest purity agreed well with the experimental carbon ratio obtained from the effects of operating variables.

Conclusions

The effects of carbon-to-zeolite ratio on the seven-step two-bed PSA processes using activated carbon and zeolite 5A were studied to produce high purity H_2 product from COG. To develop the model, the layered bed was assumed to consist of two independent beds with a single adsorbent in each. The predicted results by a mathematical model including mass, energy, and momentum balances agreed well with the experimental results.

While the product purity of a layered bed process was not between the limits of two single adsorbent bed processes due to the synergistic effects of two adsorbents, the recovery of a layered bed process was between the limits of two single-adsorbent bed processes. In this experimental range, the carbon-to-zeolite ratio to improve purity moved to a lower ratio with an increase in the adsorption pressure and the purge rate and with a decrease in the feed rate. Under the operating condition producing a high purity H_2 product, the main impurities in the zeolite-rich bed process were CO and N_2, while N_2 became a major impurity in the product as the carbon-to-zeolite ratio increased. In the case of the two-bed H_2 PSA system used in the present study, the operating conditions for obtaining 99.99+% high purity H_2 product were 11 atm adsorption pressure, 7 LSTP/min feed rate, and 0.7 LSTP/min purge rate.

The temperature variations in the bed showed well the inflection or plateau caused by the roll-up phenomenon in the bed. The result of the dynamics of adsorption through temperature variations agreed well with the carbon-to-zeolite ratio obtained from the effects of operating variables. Especially, the temperature variations of the layered bed process with 0.5 carbon-to-zeolite ratio showed an intermediate behavior of the single-adsorbent bed processes.

Since every component had its own front velocity at each layer, carbon-to-zeolite ratio affected product purity at a given recovery or throughput. Even though N_2 was a minor impurity in coke oven gas, controlling the leading wavefront of N_2 played a very important role in obtaining a high purity product and in determining the optimum carbon-to-zeolite ratio of a PSA process for high purity H_2 recovery. As a result, to obtain high product purity, it was very important to find out the superposing configuration of the adsorbents.

Acknowledgment

The financial assistance and support of Sunkyong Engineering & Construction Limited and R&D Management Center for Energy and Resources are gratefully acknowledged.

Notation

A = cross-sectional area, m^2
B = Langmuir-Freundlich isotherm parameter, atm^{-1}
C_p = heat capacity, J/kg·K
h = heat-transfer coefficient, J/m²·s·K
k_g = thermal conductivity of fluid, J/m·s·K
k_s = thermal conductivity of particle, J/m·s·K
n = Langmuir-Freundlich isotherm parameter
P = pressure, atm
Pr = Prandtl number, $(C_p)_g \mu/k_g$
q_m = Langmuir-Freundlich isotherm parameter, mol/kg
$\bar{q}$ = volume-averaged adsorbed phase concentration, mol/kg
q^* = equilibrium adsorbed phase concentration, mol/kg
Q = average isosteric heat of adsorption, J/mol
R = radius, m
Re = Reynolds number, $\rho_g \nu(2R_p)/\mu$
Sc = Schumidt number, $\mu\rho_g/D_m$
t = time, s
t_s = stoichiometric breakthrough time, s
T = solid phase and gas phase temperature, K
T_{atm} = ambient temperature, K
u = interstitial velocity, m/s
y = mole fraction in gas phase
z = axial position in an adsorption bed, m
α = total void fraction
ϵ = interparticle void fraction
μ = viscosity, m/kg·s
ρ = density, m^3/kg

Subscripts

B = bed
i = component i
p = pellet
g = gas phase
s = solid phase
w = wall

Literature Cited

Chlendi, M., D. Tondeur, and F. Rolland, ''A Method to Obtain a Compact Representation of Process Performances from a Numerical Simulator: Example of Pressure Swing Adsorption for Pure Hydrogen Production,'' *Gas Sep. Purif.*, **9**, 125 (1995).

Chou, C.-T., and W.-C. Huang, ''Simulation of a Four-Bed Pressure Swing Adsorption Process for Oxygen Enrichment,'' *Ind. Eng. Chem. Res.*, **33**, 1250 (1994).

Doong, S. J., and R. T. Yang, ''Bulk Separation of Multicomponent Gas Mixtures by Pressure Swing Adsorption: Pore/Surface Diffusion and Equilibrium Model,'' *AIChE J.*, **37**, 1027 (1986).

Farooq, S., M. M. Hassan, and D. M. Ruthven, ''Heat Effects in Pressure Swing Adsorption Systems,'' *Chem. Eng. Sci., 43, 1017 (1998)*.

Kikkinides, E. S., R. T. Yang, and S. H. Cho, ''Concentration and Recovery of CO_2 from Flue Gas by Pressure Swing Adsorption,'' *Ind. Eng. Chem. Res.*, **32**, 2714 (1993).

Kim, W. G., J. Yang, S. Han, C. Cho, C.-H. Lee, and H. Lee, ''Experimental and Theoretical Study on H_2/CO_2 Separation by a Five-Step One-Column PSA Process,'' *Korean J. Chem. Eng.*, **12**, 503 (1995).

Kumar, R., ''Pressure Swing Adsorption Process: Performance Optimum and Adsorbent Selection,'' *Ind. Eng. Chem. Res.*, **33**, 1600 (1994).

Kunii, D., and J. M. Smith, ''Heat Transfer Characteristics of Porous Rocks,'' *AIChE J.*, **6**, 71 (1960).

Liow, J.-L., and C. N. Kenney, ''The Backfill Cycle of the Pressure Swing Adsorption Process,'' *AIChE J.*, **36**, 53 (1990).

Lu, Z. P., J. M. Loureiro, A. E. Rodrigues, and M. D. LeVan, ''Pressurization and Blowdown of Adsorption Beds—II. Effect of the Momentum and Equilibrium Relations on Isothermal Operations,'' *Chem. Eng. Sci.*, **48**, 1699 (1993).

Malek, A., and S. Farooq, ''Kinetics of Hydrocarbon Adsorption on Activated Carbon and Silica Gel,'' *AIChE J.*, **43**, 761 (1997).

Ruthven, D. M., S. Farooq, and K. S. Knaebel, *Pressure Swing Adsorption*, VCH Publishers, New York (1994).

Suzuki, M., *Adsorption Engineering*, Elsevier, Amsterdam (1990).

Wakao, N., and T. Funazkri, ''Effect of Fluid Dispersion Coefficients on Particle-to-Fluid Mass Transfer Coefficients in Packed Beds,'' *Chem. Eng. Sci.*, **33**, 1375 (1978).

Yagi, S., D. Kunii, and N. Wakao, ''Studies on Axial Effective Thermal Conductivities in Packed Beds,'' *AIChE J.*, **6**, 543 (1960).

Yang, R. T., *Gas Separation by Adsorption Processes*, Butterworths, Boston (1987).

Yang, J., C. Cho, K. Baek, and C.-H. Lee, ''Comparison of One-Bed and Two-Bed H_2 PSA Using Zeolite 5A,'' *HWAHAK KONGHAK*, **35**, 545 (1997a).

Yang, J., J.-W. Chang, and C.-H. Lee, ''Separations of Hydrogen Mixtures by a Two-Bed Pressure Swing Adsorption Process Using Zeolite 5A,'' *Ind. Eng. Chem. Res.*, **36**, 2789 (1997b).

Yang, J., M.-W. Park, J.-W. Chang, and C.-H. Lee, ''Effects of Pressure Drop in a PSA Process,'' *Korean J. Chem. Eng.*, **15**, 211 (1998).

Yang, J., and C.-H. Lee, ''Adsorption Dynamics of a Layered Bed PSA for H_2 Recovery from Coke Oven Gas,'' *AIChE J.*, **44**, 1325 (1998).

Manuscript received July 27, 1998, and revision received Nov. 12, 1998.